

CHAPTER 8

TECHNIQUES FOR DETERMINING ATMOSPHERIC PARAMETERS

8.1 Total Water Vapour Estimation

8.1.1 Split Window Method

The split window method can be used to specify total water vapour concentration from clear sky 11 and 12 micron brightness temperature measurements. In the previous derivation in section 7.2, it was shown that for a window channel

$$u_s = \frac{T_{bw} - T_s}{k_w (\bar{T}_w - T_s)} .$$

Obviously, the accuracy of the determination of the total water vapour concentration depends upon the contrast between the surface temperature, T_s , and the effective temperature of the atmosphere,

\bar{T}_w . In an isothermal situation, the total precipitable water vapour concentration is indeterminate. The split window approximation allows us to write

$$T_s = \frac{k_{w2} T_{bw1} - k_{w1} T_{bw2}}{k_{w2} - k_{w1}} ,$$

and if we express \bar{T}_w as proportional to T_s

$$\bar{T}_w = a_w T_s ,$$

then a solution for u_s follows:

$$\begin{aligned} u_s &= \frac{T_{bw2} - T_{bw1}}{(\alpha_{w1}-1)(k_{w2} T_{bw1} - k_{w1} T_{bw2})} \\ &= \frac{T_{bw2} - T_{bw1}}{\beta_1 T_{bw1} - \beta_2 T_{bw2}} . \end{aligned}$$

The coefficients β_1 and β_2 can be evaluated in a linear regression analysis from prescribed temperature and water vapour profile conditions coincident with in situ observations of u_s . The weakness of the method is due to the time and spatial variability of α_w and the insensitivity of a stable lower atmospheric state when $T_{bw1} \sim T_{bw2}$ to the total precipitable water vapour concentration.

8.1.2 Split Window Variance Ratio

Following the procedure outlined for the split window moisture correction for SST of Chapter 6, we now develop the technique known as the Split Window Variance Ratio for estimating the total precipitable water vapour in an atmospheric column over one fov. Recall that for atmospheric windows with minimal moisture absorption, we write

$$I_w = B_{sw} (1 - k_w u_s) + k_w u_s \bar{B}_w .$$

Consider neighbouring fovs and assume that the air temperature is invariant, then the gradients can

be written

$$\Delta I_w = \Delta B_{sw} (1 - k_w u_s)$$

where Δ indicates the differences due to different surface temperatures in the two fovs. Convert to brightness temperatures with a Taylor expansion with respect to one of the surface temperatures, so that

$$[I_w(\text{fov1}) - I_w(\text{fov2})] = [B_{sw}(\text{fov1}) - B_{sw}(\text{fov2})](1 - k_w u_s)$$

$$[T_w(\text{fov1}) - T_w(\text{fov2})] = [T_s(\text{fov1}) - T_s(\text{fov2})](1 - k_w u_s) .$$

Using the split windows we can arrive at an estimate for u_s in the following way. Write the ratio

$$\frac{1 - k_{w1} u_s}{1 - k_{w2} u_s} = \frac{dI_{w1} dB_{sw2}}{dI_{w2} dB_{sw1}} ,$$

$$\frac{1 - k_{w1} u_s}{1 - k_{w2} u_s} = \frac{[I_{w1}(\text{fov1}) - I_{w1}(\text{fov2})] [B_{sw2}(\text{fov1}) - B_{sw2}(\text{fov2})]}{[I_{w2}(\text{fov1}) - I_{w2}(\text{fov2})] [B_{sw1}(\text{fov1}) - B_{sw1}(\text{fov2})]}$$

$$\frac{1 - k_{w1} u_s}{1 - k_{w2} u_s} = \frac{[T_{w1}(\text{fov1}) - T_{w1}(\text{fov2})] [T_s(\text{fov1}) - T_s(\text{fov2})]}{[T_{w2}(\text{fov1}) - T_{w2}(\text{fov2})] [T_s(\text{fov1}) - T_s(\text{fov2})]}$$

$$\frac{1 - k_{w1} u_s}{1 - k_{w2} u_s} = \frac{[T_{w1}(\text{fov1}) - T_{w1}(\text{fov2})]}{[T_{w2}(\text{fov1}) - T_{w2}(\text{fov2})]} ,$$

since the surface temperature cancels out. Therefore

$$\frac{1 - k_{w1} u_s}{1 - k_{w2} u_s} = \frac{\Delta T_{w1}}{\Delta T_{w2}} ,$$

or

$$u_s = (1 - \Delta_{12}) / (k_{w1} - k_{w2} \Delta_{12}),$$

where Δ_{12} represents the ratio of the deviations of the split window brightness temperatures. The deviation is often determined from the square root of the variance.

The assumption in this technique is that the difference in the brightness temperatures from one fov to the next is due only to the different surface temperatures. It is best applied to an instrument with relatively good spatial resolution, so that sufficient samples can be found in an area with small atmospheric variations and measurable surface variations in order to determine the variance of the brightness temperatures accurately. The technique was suggested by the work of Chesters *et al* (1983) and Kleespies and McMillin (1986); Jedlovec (1990) successfully applied it to aircraft data with 50 meter resolution to depict mesoscale moisture variations preceding thunderstorm development.

8.1.3 Perturbation of Split Window RTE

The total precipitable water vapour and the surface temperature can be determined from split window observations of a scene. Assuming that the temperature profile is well known for a given fov (so that δT is zero), then the perturbation form of the radiative transfer equation (see section 5.8.2 of Chapter 5) can be written

$$\delta T_b = \delta T_s \left[\frac{\partial B_s}{\partial T_s} / \frac{\partial B}{\partial T_b} \right] \tau_s + \delta u_s \int_0^{p_s} \frac{\partial \tau}{\partial u} \left[\frac{\partial B}{\partial p} / \frac{\partial B}{\partial T_b} \right] dp$$

which reduces to the form

$$\delta T_b = a \delta T_s + b \delta u_s .$$

where a and b are calculable from the initial guess. The split window offers two equations and the two unknowns T_s and u_s are readily solved.

This technique is very dependent on the accurate absolute calibration of the instrument.

8.1.4 Microwave Split Window Estimation of Atmospheric Water Vapor and Liquid Water

One can derive atmospheric water information from channels with frequencies below 40 GHz in the microwave spectrum. The 22.2 GHz channel has modest water vapor sensitivity and the 31.4 GHz channel has window characteristics; the two together are considered the microwave split window (analogous to the 11 and 12 micron infrared split window). Recalling the microwave form of the radiative transfer equation,

$$T_{b\lambda} = \epsilon_{\lambda s} T_s(p_s) \tau_{\lambda}(p_s) + \int_0^{p_s} T(p) F_{\lambda}(p) \frac{\partial \tau_{\lambda}(p)}{\partial \ln p} d \ln p$$

where

$$F_{\lambda}(p) = \left\{ 1 + (1 - \epsilon_{\lambda}) \left[\frac{\tau_{\lambda}(p_s)}{\tau_{\lambda}(p)} \right]^2 \right\} ,$$

one can write for the microwave windows

$$T_{b\lambda} = \epsilon_{\lambda s} T_s \tau_{\lambda s} + T_A [1 - \tau_{\lambda s} - (1 - \epsilon_{\lambda s}) \tau_{\lambda s}^2 + (1 - \epsilon_{\lambda s}) \tau_{\lambda s}]$$

where T_A represents an atmospheric mean temperature. Using $\tau_{\lambda s} \sim 1 - a_{\lambda}$ and $\tau_{\lambda s}^2 \sim 1 - 2a_{\lambda}$ in the window regions (where water absorption a_{λ} is small), this reduces to

$$T_{b\lambda} = \epsilon_{\lambda s} T_s \tau_{\lambda s} + T_A [1 - \epsilon_{\lambda s} \tau_{\lambda s} - \tau_{\lambda s}^2 + \epsilon_{\lambda s} \tau_{\lambda s}^2] ,$$

$$T_{b\lambda} = \epsilon_{\lambda s} T_s (1 - a_{\lambda}) + T_A [1 - \epsilon_{\lambda s} (1 - a_{\lambda}) - (1 - 2a_{\lambda}) + \epsilon_{\lambda s} (1 - 2a_{\lambda})] ,$$

$$T_{b\lambda} = \epsilon_{\lambda s} T_s (1 - a_{\lambda}) + a_{\lambda} T_A [2 - \epsilon_{\lambda s}] .$$

But for low layers of moisture detected in the split window $T_s \sim T_A$, so

$$T_{b\lambda} = \epsilon_{\lambda s} T_s + 2 a_{\lambda} T_s [1 - \epsilon_{\lambda s}] .$$

Writing $\tau_{\lambda s} = \tau_{\lambda s}(\text{liquid}) \tau_{\lambda s}(\text{vapor}) \sim [1 - Q/Q_0] [1 - U/U_0]$, where Q is the total liquid concentration with respect to reference Q_0 and U is the total vapor concentration with respect to reference U_0 , we

get

$$T_{b\lambda} = \epsilon_{\lambda s} T_s + 2 T_s [1 - \epsilon_{\lambda s}] [Q/Q_0 + U/U_0].$$

If $\epsilon_{\lambda s}$ and T_s are known, then measurements in the microwave split window offer solutions for Q and U (2 equations and 2 unknowns). Over oceans where the surface temperature and emissivity are reasonably well known and uniform, Q and U can be determined within 10%; over land reliable solutions remain elusive.

8.2 Total Ozone Determination

Ozone is an important atmospheric constituent found in the atmosphere between 10 and 50 km above the earth's surface. Because it absorbs ultraviolet rays from the sun, ozone protects man from the harmful effects of ultraviolet radiation. Also, ozone is a prime source of thermal energy in the low stratosphere and has been shown to be a useful tracer for stratospheric circulation. Prabhakara *et al* (1970) have exploited remote sensing of the total ozone using satellite infrared emission measurements and their studies reveal a strong correlation between the meridional gradient of total ozone and the wind velocity at tropopause levels. Shapiro *et al* (1982) have indicated a possibility to predict the position and intensity of jet streams using total ozone measured by satellite.

Recently, there has been increased interest in atmospheric ozone, due primarily to its role in complex middle atmospheric photochemistry and the critical ecological effect associated with ozone depletion induced by anthropogenic impacts and natural processes. By means of satellite observations, the evolution of the "ozone hole" and its interannual variability can be detected and even predicted. The main satellite instruments used for monitoring ozone are the Total Ozone Monitoring Sensor (TOMS) (Bowman and Krueger 1985; McPeters *et al.* 1996; 1998) and the Solar Backscatter Ultraviolet (SBUV) spectrometer (Heath *et al.* 1975; 1978). In order to predict the evolution of ozone on time scales of a few days to a week, reliable global measurements of the three-dimensional distribution of ozone are needed. However, neither the TOMS nor the SBUV can provide measurements at night; infrared (IR) radiance measurements as well as microwave limb sounders can. This section discusses infrared detection of ozone.

8.2.1 Total Ozone from Numerical Iteration

Ma *et al* (1983) suggested a method for obtaining total ozone with high spatial resolution from the TIROS-N/NOAA series of satellites. The ozone concentration is mapped with the 9.6 μm ozone radiance observations by the High-resolution Infrared Radiation Sounder (HIRS). The meteorological inferences have a resolution of 75 km. The influence of clouds must be screened out to produce reliable ozone determinations.

Ozone concentration is related to radiance to space through the transmittance $\tau_\lambda(p)$. As shown in the water vapour profile solution, using a first order Taylor expansion of Planck function in terms of temperature and integrating the RTE by parts, yields the expression

$$T_{b\lambda} - T_{b\lambda}^{(n)} = \int_0^{p_s} [\tau_\lambda(p) - \tau_\lambda^{(n)}(p)] X_\lambda(p) dp$$

where $T_{b\lambda}$ is the measured brightness temperature, $T_{b\lambda}^{(n)}$ is the brightness temperature calculated for a n^{th} estimate of the ozone profile, $\tau_\lambda^{(n)}(p)$ is the corresponding transmittance profile, and

$$X_\lambda(p) = \left[\frac{\partial B_\lambda(T)}{\partial T} \Big|_{T=T_{av}} / \frac{\partial B_\lambda(T)}{\partial T} \Big|_{T=T_{b\lambda}} \right] \frac{\partial T(p)}{\partial \ln p}$$

Using the mathematical derivation used for water vapour retrieval, one can relate the brightness temperature measured by HIRS in the ozone 9.6 μm band to the ozone concentration, $v(p)$:

$$T_{b\lambda} - T_{b\lambda}^{(n)} = \int_0^{p_s} \ln \frac{v(p)}{v^{(n)}(p)} Z_{\lambda}^{(n)}(p) \frac{dp}{p}$$

where

$$Z_{\lambda}^{(n)}(p) = \tau_{\lambda}^{(n)}(p) \ln \tau_{\lambda}^{(n)}(p) X_{\lambda}$$

As suggested by Smith's generalized iteration solution, we assume that the correction to the ozone concentration $v(p) - v^{(n)}(p)$ is independent of p , so that

$$\frac{v(p)}{v^{(n)}(p)} = \exp \left[\frac{T_{b\lambda} - T_{b\lambda}^{(n)}}{\int_0^{p_s} \frac{dp}{Z_{\lambda}^{(n)}(p)}} \right] = \gamma_{\lambda}^n$$

Consequently, for every pressure level, one can use this iterative procedure to estimate the true ozone concentration profile

$$v^{(n+1)}(p_j) = v^{(n)}(p_j) \gamma_{\lambda}^n$$

Convergence is achieved as soon as the difference between the measured ozone brightness temperature and that calculated is less than the measurement noise level (approximately 0.2 C). The first guess ozone profile is constructed using regression relations between the ozone concentration and the infrared brightness temperature observations of stratospheric carbon dioxide emission and the microwave brightness temperatures observations of stratospheric and tropospheric oxygen emission to space. Since ozone is a prime source of thermal energy in the low stratosphere and the upper troposphere, there is excellent correlation between the ozone concentration and the brightness temperatures observed in the HIRS carbon dioxide and MSU oxygen channels. Due to the fact that ozone and temperature sounding data yield good statistics only up to 10 mb (about 30 km), above 10 mb the ozone and temperature profiles are extrapolated using the lapse rate of USA standard ozone and temperature profiles between 10 mb and 0.1 mb (up to about 50 km). Above 50 km, the ozone contribution to the outgoing radiance is negligible.

The profile shape and the vertical position of the peak ozone mixing ratio corresponding to the ozone guess profile is crucial to obtaining a satisfactory retrieval since only one ozone channel radiance in the 9.6 μm band is used. This is because the true ozone profile is assumed to have the same shape as the first guess. Therefore, to make the ozone guess profile sufficiently accurate in both shape and position of the ozone peak mixing ratio, adjustments to the vertical position and amplitude of the guess peak mixing ratio are made based on the difference between the observed brightness temperature and the calculated brightness temperature using the ozone guess profile.

8.2.2 Physical Retrieval of Total Ozone

Another approach to retrieving the total column ozone concentration is found in the perturbation form on the RTE. Assuming that the temperature and moisture profiles as well as the surface temperature are well known for a given FOV, then the perturbation form of the radiative transfer equation reduces to

$$\delta T_{\text{oz}} = \int_0^{p_s} \delta \tau \left[\frac{\partial T}{\partial \tau} / \frac{\partial B}{\partial \tau} \right] dp$$

$$\frac{\partial T}{\partial p} \frac{\partial T}{\partial T_{oz}}$$

where T_{oz} is the 9.6 μm brightness temperature. Finally, assume that the transmittance perturbation is dependent only on the uncertainty in the column of ozone density weighted path length v according to the relation

$$\delta\tau = \frac{\partial T}{\partial v} \delta v$$

Thus

$$\delta T_{oz} = \int_0^{p_s} \delta v \frac{\partial T}{\partial p} \frac{\partial \tau}{\partial v} \left[\frac{\partial B}{\partial T} / \frac{\partial B}{\partial T_{oz}} \right] dp = f[\delta v]$$

where f represents some function.

As in the profile retrieval, the perturbations are with respect to some a priori condition which may be estimated from climatology, regression, or more commonly from an analysis or forecast provided by a numerical model. In order to solve for δv from the 9.6 μm radiance observations δT_{oz} , the perturbation profile is represented in terms of the 9.6 μm weighting function (used as the basis function $\phi(p)$); so

$$\delta v = \alpha \phi$$

where α is computed from the initial guess.

Adjustments to the vertical position and amplitude of the guess peak mixing ratio are made based on the difference between the observed brightness temperature and the calculated brightness temperature using the ozone guess profile. Specifically the vertical position is adjusted by

$$\Delta p = a + b (T_{oz}^{cal} - T_{oz}^{obs})$$

where a and b are dependent on latitude and are obtained from linear regression in an independent set of conventional sounding data.

Li *et al* (2000) have applied the physical algorithm to GOES Sounder data. They start with a first guess from a statistical regression of GOES sounder radiances against ozone mixing ratio profiles. The statistical algorithm consists of the following expression:

$$\ln(O_3(p)) = A_0 + \sum_{j=1}^{15} A_j T b_j + \sum_{j=1}^{15} A'_j T b_j^2 + C_1 p_s + C_2 \sec \theta + C_3 \cos\left(\frac{M-6}{12} \pi\right) + C_4 \cos(LAT),$$

where A , A' and C are the regression coefficients, θ is the local zenith angle of GOES FOV, M is the month from 1 to 12, and LAT is the latitude of the GOES FOV, j is the GOES band index. Since the logarithm of the water vapor mixing ratio or ozone mixing ratio is more linear to the radiance than the mixing ratio in the radiative transfer equation, $\ln(O_3(p))$ is used as a predictand in the regression. Study shows that the accuracy of ozone estimates using 15 spectral bands is better than using less spectral bands. Month and latitude are used as additional predictors since

mid-stratospheric ozone is a complex function of latitude, season and temperature. In addition, atmospheric ozone variation is highly associated with stratospheric dynamics. The physical retrieval makes a modest improvement upon the regression first guess.

Figure 8.1a shows the monthly % RMSD; it is less than 8% for all months in 1998 and 1999, with a minimum in the summer. From July to September, the % RMSD is less than 5%, indicating good agreement between GOES-8 ozone estimates and TOMS ozone measurements. Figure 8.1b shows a scatter plot of co-located GOES-8 ozone estimates and TOMS ozone measurements for June 1998 and January 1999. GOES-8 ozone estimates both in summer and in winter have good correlation with TOMS measurements. Although the ozone variation in winter is larger than in summer, the GOES-8 ozone estimates capture those variations well. To ascertain the longer-term quality and tendencies of the GOES-8 ozone estimates, single-site comparisons with ground-based Dobson-Brewer measurements were performed. Figure 8.1c shows the GOES-8 total ozone estimates for Bismarck, ND (46.77°N, 100.75°W) in 1998 along with the co-located TOMS and ground-based ozone measurements. Ground-based ozone values are seen to vary from approximately 260 DU to 390 DU. Both TOMS and GOES ozone values match the range of ground-based ozone values well. However, GOES ozone estimates have larger bias and RMSD (-15.5 DU of bias and 25.4 DU of RMSD) than TOMS (-2 DU of bias and 17 DU of RMSD).

8.2.3 HIRS Operational Algorithm

An alternate approach for estimating total atmospheric column ozone follows the NOAA operational HIRS algorithm. Total ozone is separated into upper and lower stratospheric contributions. Warm ozone in the upper stratosphere would be estimated directly from the model first guess; cold ozone in the lower stratosphere is estimated directly from its effect on the 9.6 μm channel radiance. Determination of lower stratospheric ozone requires an estimate of foreground temperature T_f and background temperature T_b . T_f is estimated from the model first guess 50 mb temperature. T_b is estimated from the infrared window brightness temperature in the absence of any ozone. The effects of upper stratospheric ozone are removed from the 9.6 μm radiance value by the following extrapolation

$$R'_{oz} = [R_{oz} - A_u R(30\text{mb})] / [1 - A_u]$$

where from the model first guess we calculate

$$A_u = 0.18 \sqrt{\text{ESU}(\text{lat})}$$

$$\text{ESU} = \text{EQ}(\text{lat}) + \text{SW}$$

$$\text{EQ} = 0.9 + 1.1 \cos(\text{lat})$$

$$\text{SW} = \text{DT} [1 + \text{DT} (2 + \text{DT})] * [270 + \text{lat}] / 9000,$$

$$\text{DT} = \text{LR} * \text{WA} / 40$$

$$\text{LR} = T(60\text{mb}) - T(100\text{mb}) - 1,$$

which is the tropopause lapse rate, and

$$\text{WA} = 2 * T(60\text{mb}) - T(30\text{mb}) - 205,$$

which is the lower stratospheric temperature anomaly. Then

$$R'_{oz} = \tau_{ls} R_b - (1 - \tau_{ls}) R_f$$

where τ_{is} is the transmittance through the lower stratosphere, R_b is the radiance from the background, and R_f is the radiance from the foreground. Solving for τ_{is} yields the amount of total ozone by inverting Beer's law.

8.3 Determination of Cloud Height and Effective Emissivity

The determination of cloud heights is important for many meteorological applications, especially the estimation of the pressure-altitude of winds obtained by tracing clouds from time sequenced satellite images. Several methods for determining cloud heights using satellite data have been developed over the years. One method (Fritz and Winston, 1962) compares the infrared window channel brightness temperature with a vertical temperature profile in the area of interest to obtain the height of the cloud. This infrared window cloud height determination assumes the cloud is opaque and fills the satellite instruments field-of-view, and thus it works fine for dense stratoforms of cloud. However, it is inaccurate for semi-transparent cirrus clouds and small element cumulus clouds. A second method (Mosher, 1976; Reynolds and Vonder Haar, 1977) improves the infrared window channel estimate of cloud top height by allowing for fractional cloud cover and by estimating the cloud emissivity from visible reflectance data. Using a multiple scattering model, the visible brightness of the cloud is used to calculate the optical thickness, from which the infrared emissivity of the cloud can be computed. Although this bi-spectral method is an improvement over the first method, it is still inaccurate for semi-transparent cirrus clouds. A third method utilizes stereographic observations of clouds from two simultaneously scanning geosynchronous satellites (Hasler, 1981). These stereo height measurements depend only on straightforward geometrical relationships and offer more reliable values than the previously discussed infrared-based methods. However, the stereo method is limited to the overlap region of the two satellites and to times when simultaneous measurements can be orchestrated.

The CO₂ absorption method enables one to assign a quantitative cloud top pressure to a given cloud element using radiances from the CO₂ spectral bands. Recalling that the radiance from a partly cloudy air column region by

$$I_\lambda = \eta I_\lambda^{cd} + (1-\eta) I_\lambda^{cl}$$

where η is the fractional cloud cover, I_λ^{cd} is the radiance from the cloud obscured field of view, and I_λ^{cl} is the radiance from a clear field of view for a given spectral band λ . The cloud radiance is given by

$$I_\lambda^{cd} = \varepsilon_\lambda I_\lambda^{bcd} + (1-\varepsilon_\lambda) I_\lambda^{cl}$$

where ε_λ is the emissivity of the cloud, and I_λ^{bcd} is the radiance from a completely opaque cloud (black cloud). Using the RTE, we can write

$$I_\lambda^{cl} = B_\lambda(T(p_s)) \tau_\lambda(p_s) + \int_{p_s}^0 B_\lambda(T(p)) d\tau_\lambda,$$

$$I_\lambda^{bcd} = B_\lambda(T(p_c)) \tau_\lambda(p_c) + \int_{p_c}^0 B_\lambda(T(p)) d\tau_\lambda.$$

where p_c is the cloud top pressure. Integrating by parts and subtracting the two terms we get

$$I_\lambda^{cl} - I_\lambda^{bcd} = \int_{p_c}^{p_s} \tau_\lambda(p) dB_\lambda$$

therefore

$$I_{\lambda}^{cl} - I_{\lambda} = \eta \varepsilon_{\lambda} \int_{p_s}^{p_c} \tau_{\lambda}(p) dB_{\lambda},$$

where $\eta \varepsilon_{\lambda}$ is often called the effective cloud amount. The ratio of the deviations in cloud produced radiances and corresponding clear air radiances for two spectral channels, λ_1 and λ_2 , viewing the same field of view can thus be written

$$\frac{I_{\lambda_1}^{cl} - I_{\lambda_1}}{I_{\lambda_2}^{cl} - I_{\lambda_2}} = \frac{\varepsilon_{\lambda_1} \int_{p_s}^{p_c} \tau_{\lambda_1}(p) dB_{\lambda_1}}{\varepsilon_{\lambda_2} \int_{p_s}^{p_c} \tau_{\lambda_2}(p) dB_{\lambda_2}}$$

If the wavelengths are chosen close enough together, then $\varepsilon_1 = \varepsilon_2$, and one has an expression by which the pressure of the cloud within the field of view (FOV) can be specified.

The left side can be determined from radiances observed by the sounder (HIRS and the GOES Sounder) and clear air radiances calculated from a known temperature and moisture profile. Alternatively, the clear air radiances could be provided from spatial analyses of HIRS or GOES Sounder clear sky radiance observations. The right side is calculated from known temperature profile and the profiles of atmospheric transmittance for the spectral channels as a function of P_c , the cloud top pressure. The optimum cloud top pressure is determined when the absolute difference [right $(\lambda_1, \lambda_2,)$ - left $(\lambda_1, \lambda_2, P_c)$] is a minimum.

These are two basic assumptions inherent in this method: (a) the cloud has infinitesimal thickness; and (b) the cloud emissivity is the same for the two spectral channels. The maximum possible error caused by assumption (a) is one-half the cloud thickness. Errors approaching one-half the cloud thickness occur for optically thin clouds (integrated emissivity roughly less than .6); for optically thick clouds (integrated emissivity roughly greater than .6) the error is small, typically one-fourth the cloud thickness or less. Errors due to assumption (b) can be minimized by utilizing spectrally close channels.

Once a cloud height has been determined, an effective cloud amount can be evaluated from the infrared window channel data using the relation

$$\eta \varepsilon_w = \frac{I_w - I_w^{cl}}{B_w(T(p_c)) - I_w^{cl}}$$

where w represents the window channel wavelength, and $B_w(T(p_c))$ is the window channel opaque cloud radiance.

Using the ratios of radiances of the three to four CO_2 spectral channels on the polar or geostationary sounder, two to three separate cloud top pressures can be determined (for example 14.2/14.0 and 14.2/13.3). If $(I_{\lambda} - I_{\lambda}^{cl})$ is within the noise response of the instrument (roughly $1 \text{ mw/m}^2/\text{ster/cm}^{-1}$) the resulting p_c is rejected. Using the infrared window and the two cloud top pressures, two effective cloud amount determinations are made. To select the most representative cloud height P_{ck} , the algorithm checks the differences between the observed values of $(I_{\lambda} - I_{\lambda}^{cl})$ and those calculated from the radiative transfer equations for the two possible cloud top pressures and effective cloud amounts,

$$[(I - I^{cl})_{\lambda} - \eta \varepsilon_k \int_{p_s}^{p_{ck}} \tau_{\lambda} dB_{\lambda}] = M_{\lambda k}.$$

P_{ck} is chosen when

$$\sum_{\lambda=1} M_k^2$$

is a minimum, where the sum is over the CO₂ channels needed to derive the cloud top pressure values.

If neither ratio of radiances (14.2/14.0 or 14.0/13.3) can be reliably calculated because the cloud induced radiance difference ($I - I^c$) is within the instrument noise level, then a cloud top pressure is calculated directly for the sounder observed 11.2 μm infrared window channel brightness temperature and the temperature profile. In this way, all clouds can be assigned a cloud top pressure either by CO₂ absorption or by infrared window calculations.

Menzel *et al* (1983) utilized the CO₂ absorption method to make several comparisons of cloud heights determined by different techniques; the comparisons were randomly made over several different cloud types including thin cirrus clouds. The CO₂ heights were found to be reliable within about a 50 mb root mean square deviation of other available height determinations. The CO₂ heights produced consistently good results over thin cirrus where the bi-spectral heights were inconsistent. This is demonstrated in Fig. 8.2, where bi-spectral and CO₂ heights are plotted along a cirrus anvil blowing off the top of a thunderstorm at 1348 GMT 14 July 1982 over western Missouri and eastern Kansas. As one moves away from the dense cumulus clouds towards the thin cirrus, the CO₂ absorption method maintains high altitudes while the bi-spectral method frequently underestimates the altitude by varying amounts depending on the thinness of the cirrus clouds.

The considerable advantage of the CO₂ absorption method is that it is not dependent on the fractional cloud cover or the cloud emissivity (in fact, the effective cloud amount is a by-product of the calculations).

8.4 Geopotential Height Determination

The geopotential Φ at any point in the atmosphere is defined as the work that must be done against the earth's gravitational field in order to raise a mass of 1 kg from sea level to that point. In other words, Φ is the gravitational potential for unit mass. The units of geopotential are 1 kg^{-1} or $\text{m}^2 \text{ s}^{-2}$. The force (in newtons) acting on 1 kg at height z above sea level is numerically equal to g . The work (in joules) in raising 1 kg from z to $z+dz$ is $g dz$; therefore,

$$d\Phi = g dz = -\alpha dp$$

where α is the reciprocal of the density of air. The geopotential $\Phi(z)$ at height z is thus given by

$$\Phi(z) = \int_0^z g dz$$

where the geopotential $\Phi(0)$ at sea level ($z = 0$) has, by convention, been taken as zero. It should be emphasized that the geopotential at a particular point in the atmosphere depends only on the height of that point and not on the path through which the unit mass is taken in reaching that point. The work done in taking a mass of 1 kg from point A with geopotential Φ_A to point B with geopotential Φ_B is $\Phi_B - \Phi_A$.

We can also define a quantity called the geopotential height Z as

$$Z = \frac{\Phi(z)}{g_0} = \frac{1}{g_0} \int_0^z g dz$$

where g_0 is the globally averaged acceleration due to gravity at the earth's surface (taken as

9.8 ms^{-2}). Geopotential height is used as the vertical coordinate in most atmospheric applications in which energy plays an important role. It can be seen from Table 8.1 that the values of z and Z are almost the same in the lower atmosphere where $g_0 \sim g$.

From the ideal gas law and the hydrostatic equation, we are able to write

$$\frac{dp}{dz} = -\frac{\rho g}{RT}$$

so that

$$\Phi_2 - \Phi_1 = -R \int_{p_1}^{p_2} \frac{dp}{T}$$

or

$$Z_2 - Z_1 = \frac{R}{g_0} \int_{p_2}^{p_1} T \frac{dp}{p}$$

Therefore, having derived a temperature profile from sounding radiance measurements, it is possible to determine geopotential heights (or thicknesses). It is readily apparent that the thickness of the layer between any two pressure levels p_2 and p_1 is proportional to the mean temperature of the layer; as T increases the air between the two pressure levels expands so that the layer becomes thicker.

Geopotential heights and thicknesses are being processed routinely from GOES soundings. Comparison with conventional radiosonde and dropwindsonde determinations for 1982-83 are shown in Table 8.2 for 1982-83. Most comparisons were made with the raobs at 1200 GMT wherever GOES soundings were sufficiently close in space and time (within approximately two hours and 100 km). Thickness derived from GOES temperature soundings showed a mean difference of only 10-30 metres when compared with raobs and 5-10 metres when compared with dropsondes.

Geopotential thickness are also routinely evaluated from the TIROS polar orbiters, but here the 850-500 and 850-200 mb layers are estimated from a linear combination of the four MSU brightness temperature observations. Regression coefficients are determined from an analysis of radiosonde data. The 850-500 and 850-200 mb thicknesses are useful for weather forecasting, since contour analyses of these quantities describe the direction and speed of the circulation at mid-tropospheric and jet stream levels, respectively. The accuracies of the MSU derived thicknesses are comparable to the accuracies experienced with the GOES derived heights and thicknesses. Figure 8.3 shows an example comparison of the NOAA-6 MSU estimates of the 850-500 and 850-200 mb thickness patterns with those obtained from radiosonde observations. The patterns are very similar.

8.5 Microwave Estimation of Tropical Cyclone Intensity

It has been observed that the upper tropospheric temperature structure of tropical cyclones is characterized by a well-defined warm temperature anomaly at upper levels in well-developed storms. An intense tropical cyclone with an eye produced by subsidence within the upper tropospheric anticyclone develops a warm core due to adiabatic warming. One theory is the warm air produced by subsidence within the eye is entrained into the eye wall where strong upward motions transport this warmer air to high levels where it then diverges outward away from the eye region.

It has been shown to be possible to monitor the intensity of tropical cyclones as categorized by its surface central pressure and maximum sustained wind speed at the eye wall with satellite microwave observations. The relationship between surface pressure and the intensity of

the warm core comes from the ideal gas law and the hydrostatic equation

$$\frac{dp}{p} = - \frac{g}{RT} dz$$

or

$$\ln \left(\frac{p_s}{p_t} \right) = \frac{g}{R} \int_0^{z_t} \frac{dz}{T}$$

where p_s is the surface pressure and p_t and z_t are the pressure and height of some level which is undisturbed by the tropical cyclone below. Thus, the surface pressure is inversely related to the temperature of the column of air above. Observations show that the transition between the lower level cyclone and upper level anti-cyclone occurs in the vicinity of 10 km. Applying the above equation at the eye and its environment we find

$$\ln \left(\frac{p_s^{\text{eye}}}{p_t} \right) = \frac{g}{R} \frac{z_t}{T_{\text{av}}^{\text{eye}}}$$

and

$$\ln \left(\frac{p_s^{\text{env}}}{p_t} \right) = \frac{g}{R} \frac{z_t}{T_{\text{av}}^{\text{env}}}$$

where T_{av} is the mean temperature of the column between the surface and the undisturbed pressure level. Combining these expressions we can write

$$p_s^{\text{eye}} = p_s^{\text{env}} \exp \left[- \frac{gz_t}{R} \left(\frac{T_{\text{av}}^{\text{eye}} - T_{\text{av}}^{\text{env}}}{T_{\text{av}}^{\text{eye}} T_{\text{av}}^{\text{env}}} \right) \right]$$

Using $z_t = 10$ km and setting $T_{\text{av}}^{\text{eye}} T_{\text{av}}^{\text{env}} \sim (250 \text{ K})^2$ then

$$p_s^{\text{eye}} \sim p_s^{\text{env}} \exp [-.0055 \Delta T_{\text{av}}]$$

$$\sim p_s^{\text{env}} [1 - .0055 \Delta T_{\text{av}}].$$

Assuming $p_s^{\text{env}} \sim 1000$ mb, then

$$p_s^{\text{eye}} - 1000 = - 5.5 \Delta T_{\text{av}}$$

so that a 55 mb surface pressure depression is approximately associated with a 10 C contrast between the mean temperatures of the cyclone eye and its environment.

It has been found that the tropical cyclone warm core is usually strongest at about 250 mb. In addition, the amplitude of the upper tropospheric temperature anomaly is well-correlated with the amplitude of the mean temperature of the tropospheric column below 10 km. Therefore, the deviation of the temperature field at 250 mb provides a measure of the strength of the warm core, which then is correlated to storm surface intensity. Furthermore, a correlation should also exist for maximum surface winds as they are directly related to the pressure field (although not pure gradient winds because of frictional effects).

In the work of Velden *et al* (1984), ΔT_{250} is compared to observed surface central pressure and maximum winds, where ΔT_{250} is the gradient of the 250 mb temperature field defined as the core temperature minus the average environmental temperature at a six degree radius from the storm core. Linear regression is used to find a best fit for the data. After studying over 50 cases, they found that the standard error of estimates for the central pressure and maximum wind are 6 mb and 10 knots, respectively. Figure 8.4 shows these results. Figure 8.5 shows a comparison of National Hurricane Centre (now called Tropical Prediction Center) versus satellite estimates of the central surface pressure and maximum sustained wind speed for the duration of Hurricane Barry. TOVS microwave intensity estimates continue to augment existing methods.

8.6 Satellite Measure of Atmospheric Stability

One measure of the thermodynamic stability of the atmosphere is the total-totals index

$$TT = T_{850} + TD_{850} - 2T_{500}$$

where T_{850} and T_{500} are the temperatures at the 850- and 500-mb levels, respectively, and TD_{850} is the 850-mb level dew point. TT is traditionally estimated from radiosonde point values. For a warm moist atmosphere underlying cold mid-tropospheric air, TT is high (e.g., 50-60 K) and intense convection can be expected. There are two limitations of radiosonde derived TT: (a) the spacing of the data is too large to isolate local regions of probable convection; and (b) the data are not timely since they are available only twice per day.

If we define the dew point depression at 850 mb, $D_{850} = T_{850} - TD_{850}$, then

$$TT = 2(T_{850} - T_{500}) - D_{850}.$$

Although point values of temperature and dew point cannot be observed by satellite, the layer quantities observed can be used to estimate the temperature lapse rate of the lower troposphere ($T_{850} - T_{500}$) and the low level relative moisture concentration D_{850} . Assuming a constant lapse rate of temperature between the 850- and 200-mb pressure levels and also assuming that the dew point depression is proportional to the logarithm of relative humidity, it can be shown from the hydrostatic equation that

$$TT = 0.1489 \Delta Z_{850-500} - 0.0546 \Delta Z_{850-200} + 16.03 \ln RH,$$

where ΔZ is the geopotential thickness in metres and RH is the lower tropospheric relative humidity, both estimated from either TIROS or GOES radiance measurements as explained earlier.

Smith and Zhou (1982) reported several case studies using this approach. Figure 8.6 shows the total-totals stability index as observed by radiosondes and infrared from TOVS data on 31 March 1981. One can see the coarse spacing of the radiosonde observations (Fig. 8.6(a)). The analysis of satellite data possesses much more spatial detail since the spacing of the data is only 75 km (Fig. 8.6(b)). There is general agreement in the high total-totals over Illinois and Missouri, but also some areas of disagreement (e.g., Nebraska). In this case, the radiosonde data are not as coherent an indicator of the region of intense convection as are the satellite data.

Also shown on the satellite TT analysis are the streamlines of the wind observed at the surface. On this occasion, it appears that the unstable air observed along the Illinois-Iowa border at 1438 GMT was advected into central Wisconsin and supported the development of a tornadic storm at 2315 GMT.

Table 8.1

**Values of the Geometric Height (z), Geopotential height (Z),
and Acceleration Due to Gravity (g) at 40 Latitude**

z(km)	Z(km)	g(ms ⁻²)
0	0	9.802
1	1.000	9.798
10	9.9869	9.771
20	19.941	9.741
30	29.864	9.710
60	59.449	9.620
90	88.758	9.531
120	117.795	9.443
160	156.096	9.327
200	193.928	9.214
300	286.520	8.940
400	376.370	8.677
500	463.597	8.427
600	548.314	8.186

Table 8.2

**Summary of Comparisons Between GOES(VAS) and Radiosonde Data
For Bermuda, San Juan and West Palm Beach
(1 August-30 November 1983)**

Parameter	Mean (VAS-RAOB)	Standard Deviation	Range	Number of Cases
Z850 (m)	7	10	-23 to 31	68
Z700	13	13	-21 to 36	67
Z500	18	19	-26 to 38	67
Z400	22	20	-37 to 66	65
Z300	30	27	-52 to 71	63
Z200	32	37	-63 to 110	62
Z500-850 (m)	12	15	-31 to 63	69
Z400-850	16	18	-42 to 50	67
Z300-850	23	26	-63 to 71	65
Z500-700	6	12	-28 to 52	68
Z400-700	10	16	-39 to 35	66
Z200-400	9	28	-78 to 60	63
Summary of Comparisons between VAS and ODW for 14-15 and 15-16 September 1982				
Parameter	Mean (VAS-RAOB)	Standard Deviation	Range	Number of Cases
Z850 (m)	-6	23	-68 to 26	42
Z700	0	22	-58 to 41	42
Z500	1	24	-56 to 44	35
Z400	2	27	-54 to 47	24
Z400-850 (m)	11	17	-16 to 45	24
Z500-850	6	14	-18 to 43	35
Z400-700	4	14	-16 to 34	24

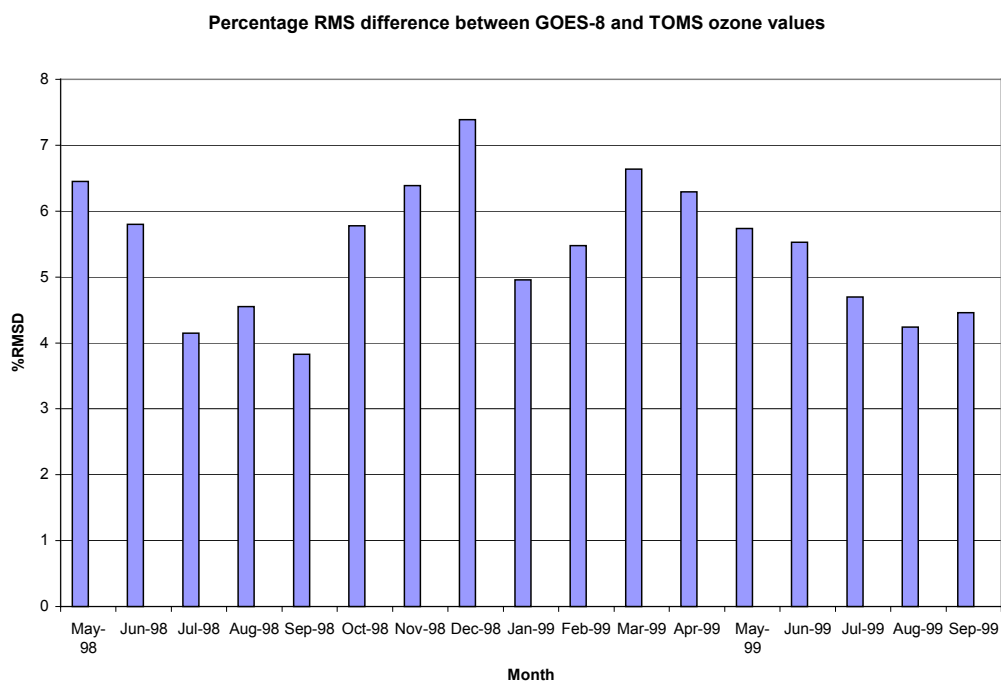
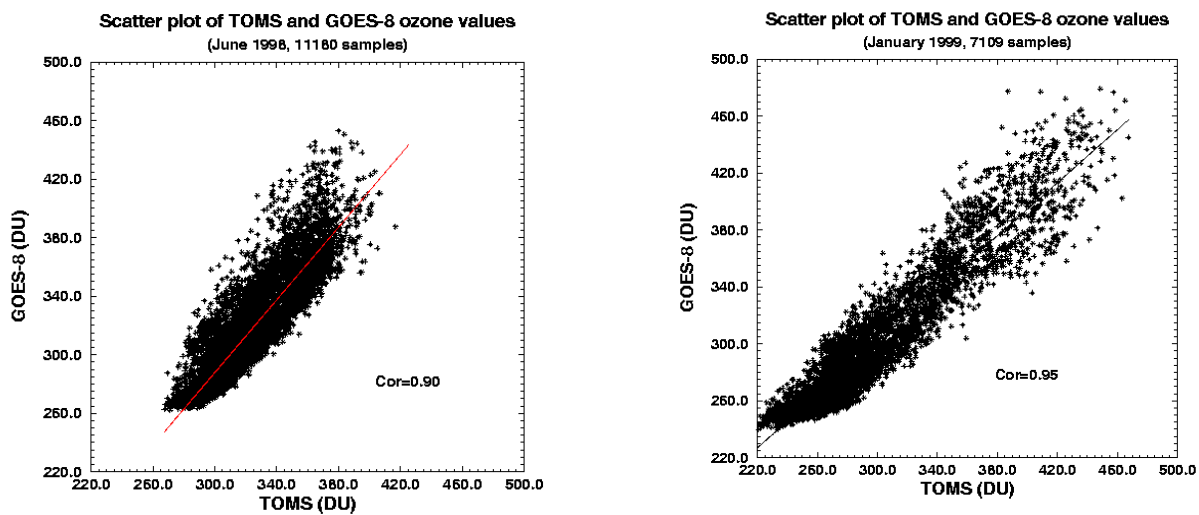


Figure 8.1a: The monthly % RMSD between the GOES-8 ozone estimates and the TOMS ozone measurements between May 1998 and September 1999.



Cor:

Cor:

Figure 8.1b: Scatter plot of co-located GOES-8 ozone estimates and the TOMS ozone measurements for June 1998 (left) and January 1999 (right).

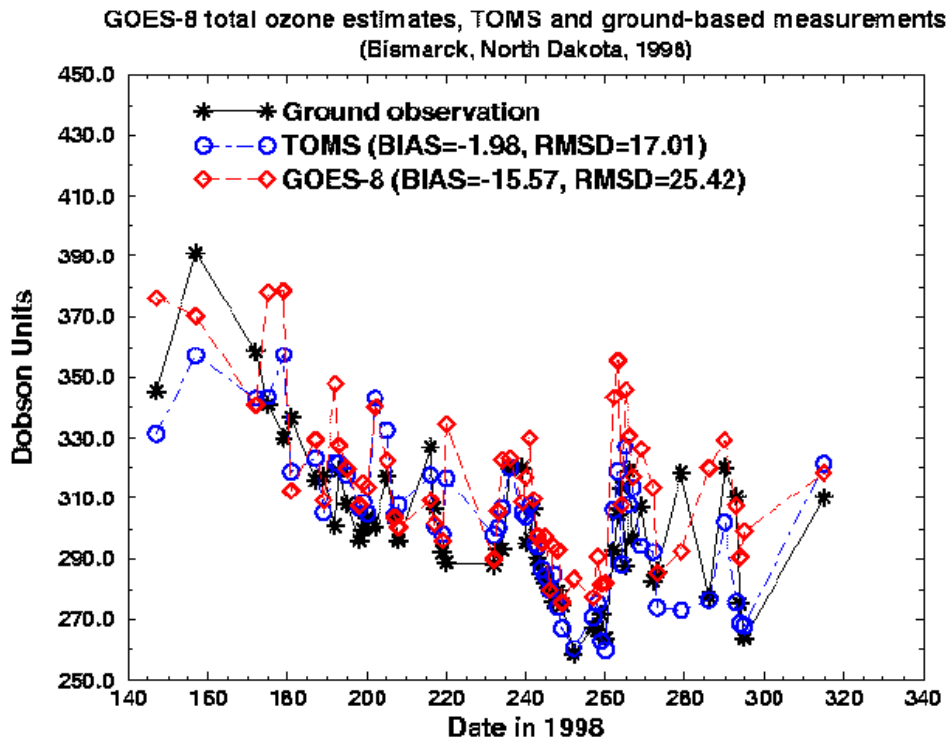


Figure 8.1c: GOES-8 total ozone estimates for Bismarck, North Dakota (46.77°N, 100.75°W) in 1998 along with the TOMS and ground-based ozone measurements.

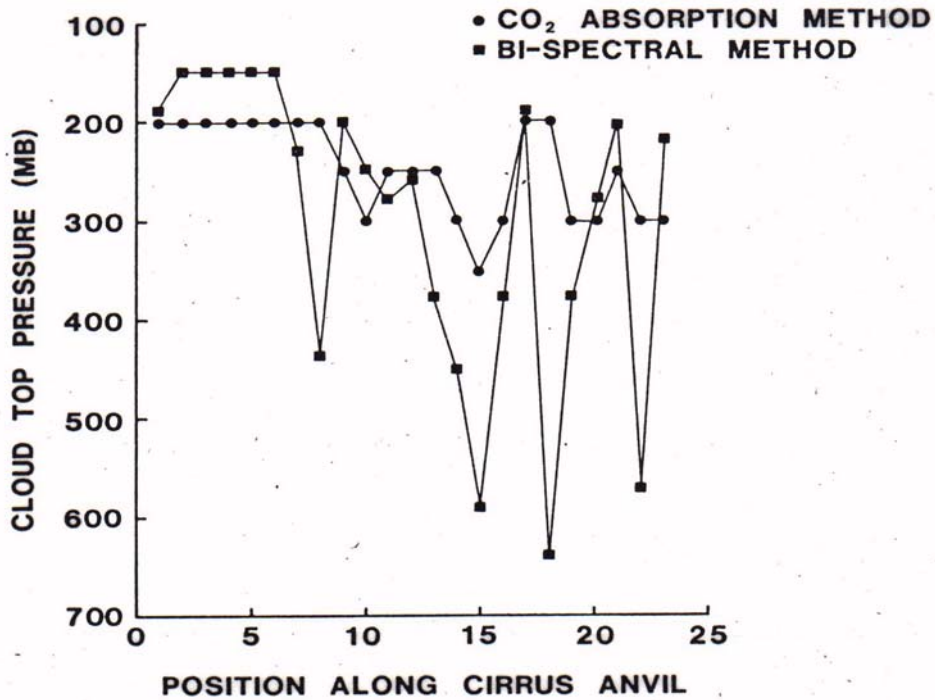


Figure 8.2: Bi-spectral and CO₂ absorption cloud-top pressures (mb) plotted versus the position along a cirrus anvil emanating from the thunderstorm over Missouri and Kansas of 1348 GMT 14 July 1982.

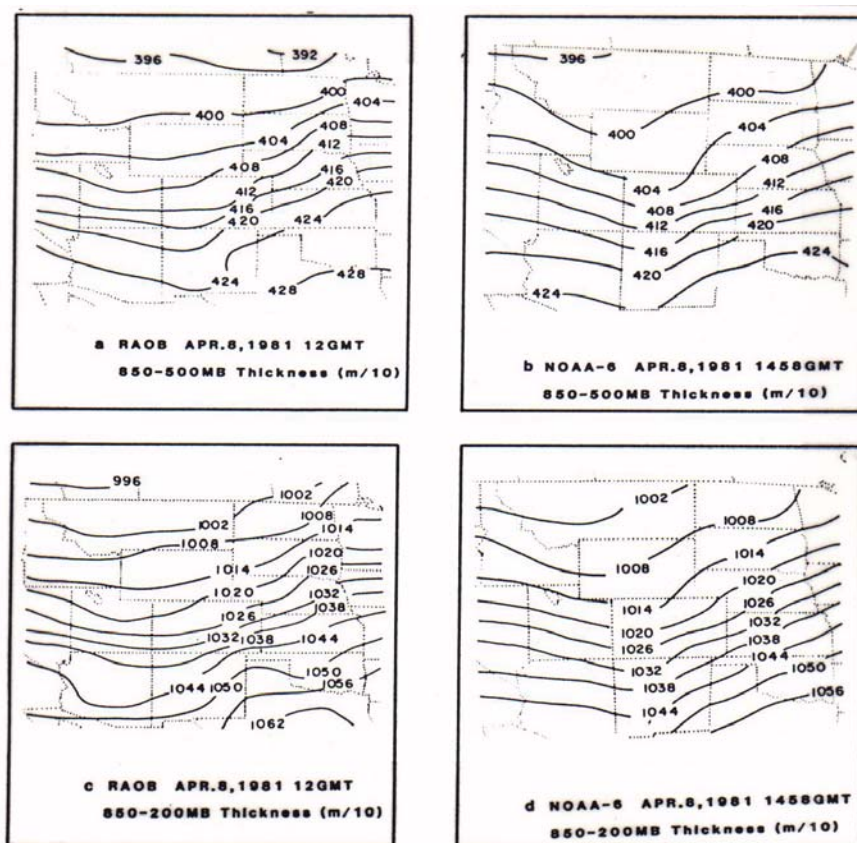


Figure 8.3: Comparison of NOAA-6 MSU estimates of 850-500 and 850-200 mb thickness patterns with those obtained from radiosonde observations.

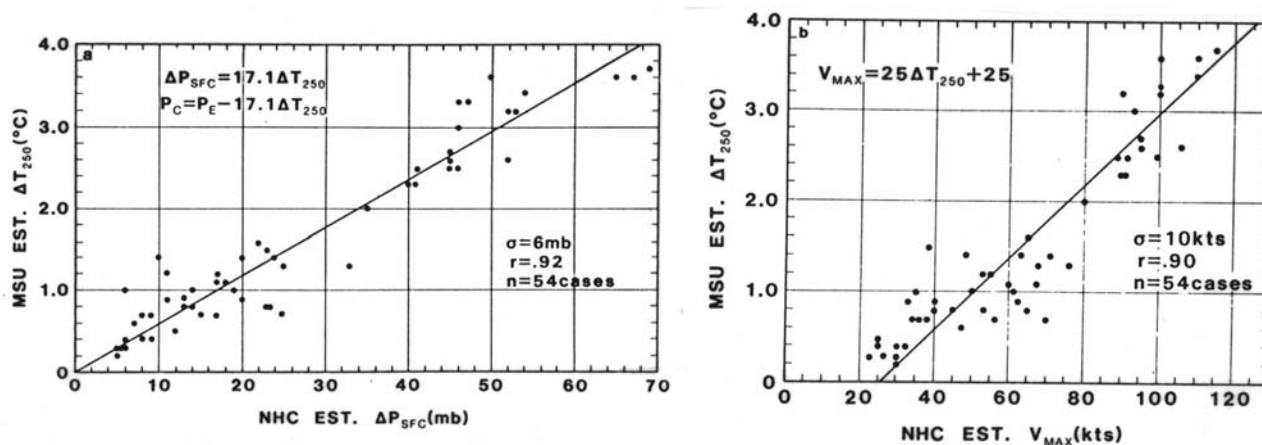


Figure 8.4: Comparison of ΔT_{250} versus the National Hurricane Centre estimated (left) central surface pressure P_C , and (right) maximum winds V_{max} . P_E is the average environmental surface pressure surrounding the storm at a 6 degree radius, n is the number of cases, r is the correlation coefficient, and σ is the standard deviation. (from Velden *et al*, 1984).

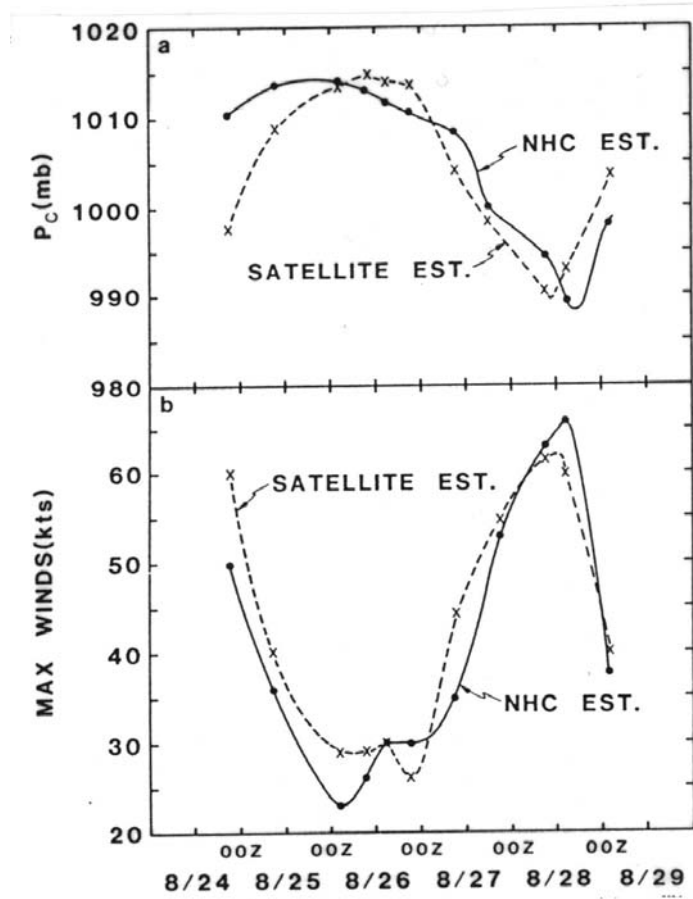


Figure 8.5: Comparison of National Hurricane Center versus satellite estimates of central surface pressure for the duration of Hurricane Barry. (from Velden *et al*, 1984).

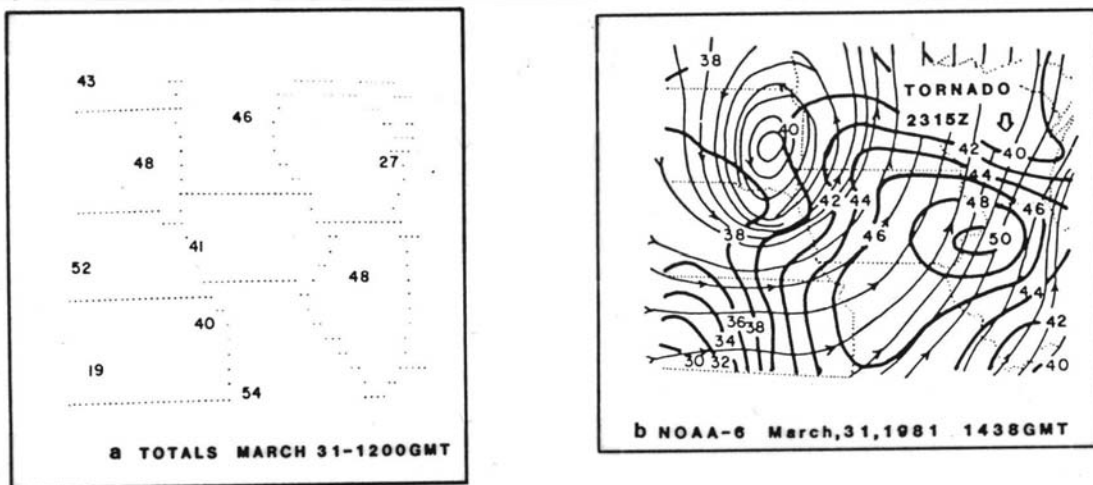


Figure 8.6: Radiosonde observations of total-totals (left) and a contour analysis (heavy lines) of NOAA-6 derived stability values with streamlines (thin lines) of the surface wind superimposed (right).